Radiation Physics and Chemistry 219 (2024) 111658

Contents lists available at ScienceDirect

Radiation Physics and Chemistry

journal homepage: www.elsevier.com/locate/radphyschem

Gamma attenuation, dose rate and exposure/absorption buildup factors of apatite–wollastonite (AW) ceramic system

Norah Alomayrah [a], Marzoqa M. Alnairi [b], Z.A. Alrowaili [c], B. Alshahrani [d], Mine Kırkbınar [e], I.O. Olarinoye [f], Halil Arslan [g], M.S. Al-Buriahi [h,*]

[a] Department of Physics, College of Science, Princess Nourah bint Abdulrahman University, P .O. Box 84428, Riyadh, 11671, Saudi Arabia
[b] Department of Physics, Umm Al-Qura University, Makkah, 24382, Saudi Arabia
[c] Department of Physics, College of Science, Jouf University, P.O.Box:2014, Sakaka, Saudi Arabia
[d] Department of Physics, Faculty of Science, King Khalid University, P.O. Box 9004, Abha, Saudi Arabia
[e] Department of Metallurgical and Materials Engineering, Faculty of Technology, Sakarya University of Applied Sciences, Sakarya, Turkey
[f] Department of Physics, School of Physical Sciences, Federal University of Technology, Minna, Nigeria
[g] Electrical and Electronics Engineering, Sakarya University of Applied Sciences, Sakarya, Turkey
[h] Department of Physics, Sakarya University, Sakarya, Turkey

ARTICLE INFO

Handling Editor: Piotr Ulanski

Keywords:
Gamma attenuation
Dose rate
Buildup factors
Apatite-wollastonite
FLUKA

ABSTRACT

Apatite-wollastonite (AW) is an important biomaterial useful in clinical practice for tissue engineering and other applications. In this research paper, AW and B_2O_3-doped AW glass ceramics (GCs) were reported and investigated deeply by means of their ability to attenuate gamma-photons. The studied samples denoted by AW, AW-10B, and AW-20B as the B_2O_3 content from 0 to 20 mol% with the step of 10. Using FLUKA and other theoretical approaches, photon interaction parameters for narrow and broad beam transmission through the AW GCs were estimated for the 15 keV–15 MeV energy range. Also, the density of the GCs increased as the B_2O_3 content increased. The mass attenuation coefficients were found to be within the ranges 0.0231–13.5659 cm^2/g, 0.0225–12.3561 cm^2/g, and 0.0220–11.1079 cm^2/g for AW, AW-10B, and AW-20B, respectively. The effective atomic number of the GCs fell within the range 11.04–17.26, 10.88–17.01, and 10.21–16.72, respectively. As the doping concentration of B_2O_3 increased, the gamma energy that the AW GCs were able to absorb decreased. The addition of B_2O_3 compromised the photon shielding competence of AW in both narrow beam and broad beam scenarios. The GCs had better photon-absorbing competence than some existing gamma-photon shields. The GCs may thus be used as photon absorbers in clinical practice or in other nuclear applications.

1. Introduction

Bioactive glasses and ceramics have become useful materials in the management of ailments affecting tissues and organs of the human biological system. Today, glasses, ceramics, and glass ceramics (GCs) with similar mineral composition as human tissues and high biocompatibility have been prepared and used for different purposes in medicine, such as dental implants, bone engineering, substitution, and regeneration (Workie et al., 2023; Oonishi et al., 1999; Al- et al., 2022a; Rammah et al., 2021). Despite the availability of different bioactive glasses and ceramics with good chemical compatibility and strong tissue-bonding abilities, the clinical applications of some of these existing biomaterials are limited. This is a result of some inherent attributes, which make them unfit for purpose (Sola et al., 2023). For instance, apatite-wollastonite (AW) glass ceramics (GCs) and hydroxyapatite (HA) are some of the best-known biomaterials for tissue reconstruction and dental implants (Workie et al., 2023). However, HA has low long-term bioactivity and osteoconductivity (Yamamuro, 2016). In addition, HA has low mechanical strength. On the other hand, AW GCs are mechanically stronger and possess higher osteoconductivity (Workie et al., 2023). Therefore, much attention has been focused on the preparation and enhancement of the attributes of AW GCs.

In an attempt to understand how the preparatory method influenced the attributes of AW GCs, many synthesis approaches were used, with each having merits and demerits. The melt-and-quench method was originally used to prepare AW GCs by Kokubo et al. (1982). The method

* Corresponding author.
E-mail address: alburiahi@sakarya.edu.tr (M.S. Al-Buriahi).

https://doi.org/10.1016/j.radphyschem.2024.111658
Received 13 November 2023; Received in revised form 6 February 2024; Accepted 29 February 2024
Available online 1 March 2024
0969-806X/© 2024 Published by Elsevier Ltd.

was adjudged good for mass production but compromises purity and a high temperature is required (Li et al., 1991). The AW GCs have also been successfully prepared using the sol-gel route, but the method was found to be unsuitable for mass production (Shih et al., 2010). Other methods have also been identified with their merits and demerits (Workie et al., 2023). Furthermore, doping AW GCs with different materials has produced tremendous changes in the features and applications of the GCs. In 2009, Li et al. (Da Li et al., 2009) discovered that doping AW GCs with Mn–Zn ferrite reduced their bioactivity and introduced new structural phases in the material (Da Li et al., 2009). Using the sol-gel method, Rattanachan et al. (2012) in 2012 prepared AW GCs doped with Zn. The analysis of the GCs showed bulk density and mechanical strength were compromised with an increase in Zn content. It was also discovered that increasing the Zn content improved chemical stability and, hence, slowed down the rate of apatite formation. Similarly, doping with Ti has been found to improve the quality of AW GCs as orthopaedic implants (Jing et al.). Ti also improved the compressive strength and chemical stability, slowed down the rate of degradation and increased the bioactivity of AW GCs (Jing et al.). Clearly, the chemical composition of AW GCs is directly linked to their bioactivity, chemical stability, strength, and other properties. Therefore, one of the ways of improving the properties and functionalities of AW GCs is by doping with appropriate material.

According to Kitsugi et al. (1992), when CaF_2 in AW GCs is partially replaced with B_2O_3, it improves the mechanical strength and the bone bonding ability of the GCs. The substitution was found to significantly affect the bone formation and bonding ability of the GC. The mechanical strength and bioactivity of other bioglasses have been found to improve after doping with B_2O_3 (Yang et al., 2012). The positive impact of B_2O_3 makes B_2O_3-doped AW GCs potentially good biomaterials for bone generation and reconstruction. In many previous studies on AW GCs, attention has been focused mainly on changes in bioactivity, structural properties, mechanical strength, tissue bonding activity, etc.; however, little attention has been paid to the radiation response. The use of gamma photons in medical procedures is well known. In addition, gamma photons are used for characterization, improving bulk properties, and sterilisation, among others (Menazea and Abdelghany, 2020; Ogundare and Olarinoye, 2016; Olarinoye and Ogundare, 2017; Świontek et al., 2021). Therefore, the possible exposure of AW GCs to gamma radiation cannot be ruled out. In order to understand and quantify the likely influence of photon irradiation, the gamma response parameters are essential (Olarinoye et al., 2020; Al- et al., 2022b; Alalawi et al., 2020; Al- et al., 2021a; Olarinoye et al., 2021; Berger, 2010; Samdani et al., 2024; Alzahrani et al., 2023a; Olarinoye et al., 2019). These parameters are often used to estimate the stability of the irradiated material in radiation environments. In addition, photon interaction parameters could be adopted to ascertain the functionality of a material in radiation fields. For example, a biomaterial with a high radiation absorption cross section could be used to shield other sensitive tissues during a photon therapy procedure. An unstable material after photon absorption could be used as a radiation detector or dosimeter. Also, a bioactive material with a similar gamma photon response as human tissue could be used as an equivalent material in radiation physics research. The benefits derivable from the parameters related to the gamma photon absorption response parameters of AW GCs are therefore invaluable to the scientific and medical communities.

In the research, B_2O_3-doped AW GCs were reported, and their ability to attenuate the gamma-photons was studied and deeply discussed. In addition, the photon interaction parameters of the GCs for a wide photon energy spectrum were obtained from Monte Carlo simulations and standard calculations. The data presented in this study are novel and would provide other perspectives on AW GCs, their properties, potential applications in medicine and other areas of radiation applications.

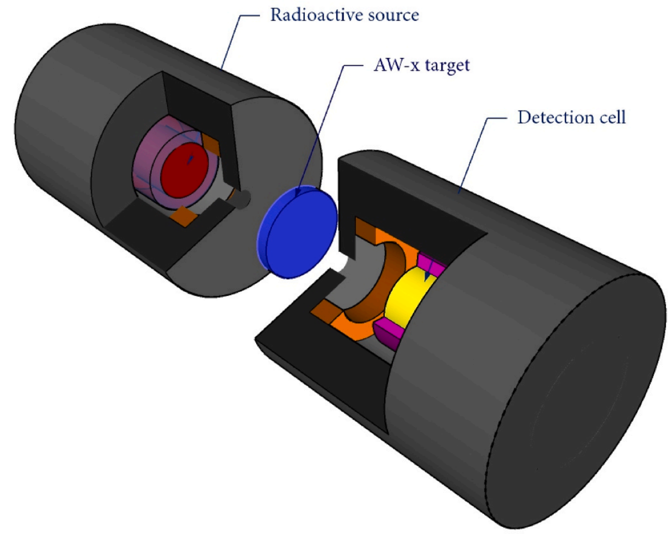

Fig. 1. FLUKA simulation setup of narrow beam γ-ray transmission geometry used for the attenuation measurements of prepared AW-*x*B sample.

2. Materials and method

Using the solid-state reaction method, AW glass ceramics doped with varying concentrations of B_2O_3 were prepared. Powdered AW and B_2O_3 (purity 99.99%) procured from Merck in Germany, were thoroughly mixed in the ratios as indicated as follows:

AW: undoped AW GCs

AW-10B: 10% B_2O_3-doped AW GCs

AW-20B: 20% B_2O_3-doped AW GCs

The B_2O_3 content was added in wt%. The components were extensively combined for 30 min using the ball milling method in order to achieve homogenous samples and a solid-state reaction. The resulting powder samples were subjected to a pressure of 250 MPa using the cold isostatic press (CIP) method to densify them. The samples were then sintered at 1000 C for 2 h in an aluminium crucible. The samples were characterized for density, using the Archimedes method, with the values of 2.905, 2.957, and 2.986 g/cm^3 for the AW, AW-10B, and AW-20B, respectively.

To obtain the gamma photon interaction parameters, first, the samples were defined using their chemical composition and density in MATERIAL card in FLUKA. Using photon beam of energies within 15 keV and 15 MeV range, transmission of gamma photons through the materials were simulated using the FLUKA Monte Carlo code using the geometry summarized in Fig. 1. Using the AW GCs' density (ρ) and thickness (t), unattenuated (N_o), and attenuated (N) beam intensities, the mass attenuation coefficients (μ/ρ) of the GCs at different energies were computed according to Equation (1).

$$\mu/\rho\ (cm^2 g^{-1}) = \frac{\ln\left(\frac{N_o}{N}\right)}{\rho t} \quad (1)$$

To validate the adopted geometry, the μ/ρ values were also estimated using the free online XCOM tool (Olarinoye et al., 2020) and compared with that obtained from FLUKA. The comparison was quantified using the deviation (in %) (Dev.%) calculated as:

$$Dev.\ (\%) = \left|\frac{(\mu/\rho)^{XCOM} - (\mu/\rho)^{FLUKA}}{(\mu/\rho)^{XCOM}}\right| \times 100 \quad (2)$$

where, $(\mu/\rho)^i$ represents the μ/ρ value obtained either FLUKA simula-

Table 1
Chemical classifications and code of the samples.

Composition (wt%)	AW	AW-10B	AW-20B
MgO	1.95	1.755	1.56
Al_2O_3	1.9	1.71	1.52
SiO_2	33.78	30.402	27.024
CaO	48.85	43.965	39.08
CaF_2	0.07	0.063	0.056
P_2O_5	13.45	12.105	10.76
B_2O_3	–	10	20

tions or XCOM data. Furthermore, photon interaction parameters such as the linear attenuation coefficient μ, half value layer (HVL), mean free path (λ), effective atomic number (Z_{eff}), and effective electron density (N_{eff}) were computed from μ/ρ using the following equations (Olarinoye et al., 2021; Berger, 2010; Samdani et al., 2024; Alzahrani et al., 2023a):

$$\mu = \rho \times \mu/\rho \quad (3)$$

$$HVL = \frac{\ln 2}{\mu} \quad (4)$$

$$\lambda = \frac{1}{\mu} \quad (5)$$

$$Z_{eff} = \frac{\sum_i f_i A_i \left(\frac{\mu}{\rho}\right)_i}{\sum_i f_j \frac{A_i}{Z_i} \left(\frac{\mu}{\rho}\right)_i} \quad (6)$$

$$N_{eff} = \frac{N_A Z_{eff}}{\langle A \rangle} \quad (7)$$

Parameters related to photon energy absorption in the GCs, including mass energy absorption coefficient ($\frac{\mu_{en}}{\rho}$), specific gamma constant Γ, and absorbed doses at different depths were estimated using data from NIST-XCOM database (Berger, 2010) and standard expressions (Samdani et al., 2024; Alzahrani et al., 2023a).

To fully describe the photon interaction processes of the AW GCs, their scattering ability were also assessed by evaluating the equivalent atomic number, energy absorption (EABF), and exposure (EBF) buildup factors using the well-known geometric projection (GP) fitting procedure. Details of the GP fitting method have been discussed severally in the literature such as (Olarinoye et al., 2019; Alzahrani et al., 2022; Al- et al., 2021b; Al- et al., 2021c; Yoshida, 2006).

3. Results and discussion

The code and chemical definition of the AW GCs samples as revealed by the XRF analysis are presented in Table 1. The pristine AW sample had five major oxides (MgO, Al_2O_3, SiO_2, CaO, and P_2O_5), and a trace amount of CaF_2 was also identified in the chemical structure of AW as expected. Upon the introduction of B_2O_3, the chemical definition of AW was altered. Increasing the concentration of B_2O_3 led to a decrease in the composition of pristine AW.

The values of $(\mu/\rho)^{XCOM}$, $(\mu/\rho)^{FLUKA}$, and *Dev*. (%) for the doped AW GCs are tabulated against energy in Table 2. The absolute values of the deviations between the two μ/ρ data were generally below 1.12%. These narrow deviations clearly showed that the FLUKA geometry (Fig. 1) adopted for the simulation approximately depicts a narrow beam transmission setup. Thus, the simulated data and consequent μ/ρ are accurate and precise.

The measure of photon interaction and transmission through a material can be expressed as μ/ρ. Higher interaction cross-sections and lower photon transmission are indicated by a higher value of μ/ρ. The simulated results showed that μ/ρ varies with energy and differs for each GC. The values of μ/ρ were found to be within the ranges 0.0231–13.5659 cm^2/g, 0.0225–12.3561 cm^2/g, and 0.0220–11.1079 cm^2/g for AW, AW-10B, and AW-20B, respectively, as shown in Table 2. In Fig. 2, the numerical values of μ/ρ and μ are plotted against photon energy (E). The figure and the values in Table 2 clearly show that the photon attenuation capacity decreases continuously as energy increases. However, the rate of decrease was higher at the lower end of the energy spectrum. In addition, there are distinctions between the values of the attenuation coefficients of the AW GCs at energy. These changes in the photon transmission abilities of the prepared samples are due to the relative dependence of photon interactions on energy and atomic differentiation. Generally, photons can interact with matter in a variety of ways, such as photoelectron creation, incoherent scattering, and

Table 2
Mass attenuation coefficient of the prepared AW-*x*B glasses via FLUKA and XCOM at different photon energies.

Energy (MeV)	AW			AW-10B			AW-20B		
	XCOM	FLUKA	Dev.%	XCOM	FLUKA	Dev.%	XCOM	FLUKA	Dev.%
0.015	13.68301	13.56593	0.856	12.45626	12.35611	0.804	11.22955	11.10788	1.083
0.02	6.00704	6.03273	0.428	5.47535	5.49994	0.449	4.94368	4.99228	0.983
0.03	1.93025	1.93524	0.259	1.76968	1.77451	0.272	1.60913	1.60601	0.194
0.04	0.91592	0.91569	0.025	0.84772	0.84728	0.053	0.77953	0.77905	0.061
0.05	0.54986	0.54404	1.057	0.51474	0.50907	1.102	0.47963	0.47453	1.065
0.06	0.38548	0.38156	1.018	0.36500	0.36120	1.042	0.34452	0.34080	1.080
0.08	0.25006	0.25116	0.440	0.24120	0.24217	0.404	0.23234	0.23341	0.460
0.1	0.19741	0.19787	0.233	0.19269	0.19288	0.098	0.18796	0.18830	0.178
0.15	0.14887	0.14907	0.135	0.14723	0.14753	0.203	0.14559	0.14586	0.186
0.2	0.12922	0.13038	0.904	0.12835	0.12949	0.890	0.12749	0.12867	0.926
0.3	0.10864	0.10953	0.810	0.10822	0.10911	0.824	0.10779	0.10865	0.794
0.4	0.09633	0.09684	0.529	0.09604	0.09655	0.529	0.09574	0.09622	0.496
0.5	0.08758	0.08806	0.551	0.08735	0.08780	0.515	0.08711	0.08761	0.574
0.6	0.08082	0.08082	0.002	0.08062	0.08062	0.007	0.08042	0.08042	0.002
0.8	0.07083	0.07109	0.368	0.07067	0.07096	0.420	0.07050	0.07078	0.392
1.0	0.06361	0.06349	0.189	0.06347	0.06335	0.192	0.06334	0.06322	0.181
1.5	0.05181	0.05158	0.456	0.05169	0.05146	0.453	0.05158	0.05135	0.450
2	0.04478	0.04457	0.451	0.04465	0.04445	0.446	0.04452	0.04433	0.443
3	0.03673	0.03640	0.890	0.03656	0.03623	0.894	0.03638	0.03606	0.897
4	0.03230	0.03201	0.892	0.03208	0.03179	0.902	0.03185	0.03156	0.912
5	0.02954	0.02929	0.868	0.02927	0.02901	0.881	0.02900	0.02874	0.885
6	0.02772	0.02752	0.728	0.02741	0.02721	0.730	0.02709	0.02689	0.744
8	0.02553	0.02542	0.439	0.02514	0.02503	0.457	0.02475	0.02464	0.467
10	0.02436	0.02425	0.447	0.02391	0.02380	0.455	0.02346	0.02335	0.466
15	0.02319	0.02309	0.432	0.02262	0.02252	0.424	0.02205	0.02196	0.407

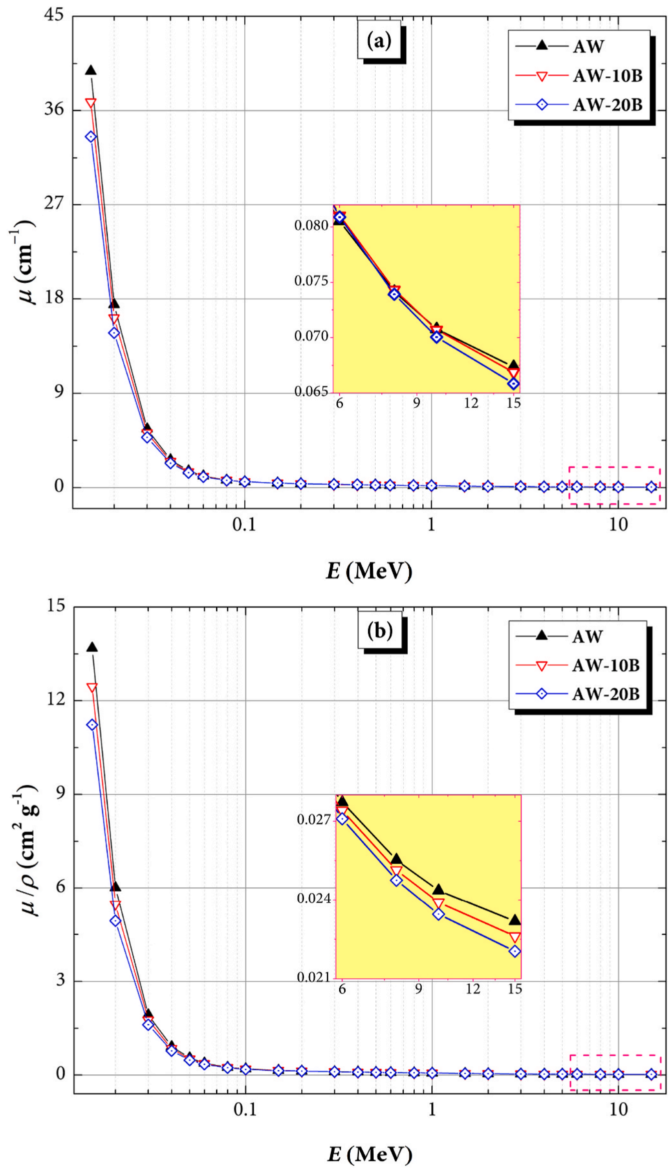

Fig. 2. Variations of (a) linear attenuation coefficient and (b) mass attenuation coefficient of the prepared AW-*x*B glasses.

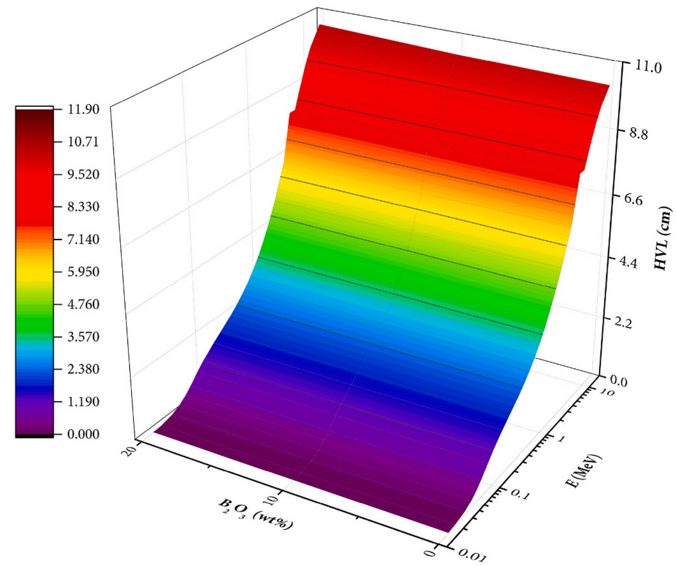

Fig. 3. Variation of half value layer (HVL) with respect to the concentration of B_2O_3 and a function of photon energy in the prepared AW-*x*B glasses.

electron-positron pair creation. The probabilities of each of these events are dependent on the number of atomic electrons available in the interacting medium and photon energy. In addition, these three interaction modes are significant in the gamma energy range presented in Table 2 and Fig. 2. Theoretically, the probability of photon interacting such that photoelectrons are produced, photons are scattered incoherently, and the creation of positron-electron pairs, represented as σ_{PE}, σ_{inc}, σ_{PEP}, respectively, have the following energy and number of electron (Z) dependences:

$$\sigma_{PE} \propto Z^5 / E^{3.5} \quad (8)$$

$$\sigma_{inc} \propto Z / EA \quad (9)$$

$$\sigma_{PEP} \propto Z^2 E \quad (10)$$

Therefore, the high but rapidly decreasing attenuation coefficients for 15 keV ≤ E ≤ 80 keV are due to the dominance of photoelectron creation. In addition, the distinctions between the attenuation coefficients of each GC (at this energy range) are a result of the differences in the number of atomic electrons (Z) available for photoelectric interaction. Therefore, it is clear that the B_2O_3-rich AW GCs present a lower number of electrons for interactions. As the energy progresses, the incoherent scattering of photons dictates the energy dependence of the attenuation coefficients. Hence, the coefficients continue their downward trend, but with less vigour as predicted by **Equation (9)**. The absence of an increase in the value of linear and mass attenuation coefficients, especially in the high energy region where pair production is usually dominant, is an indication that σ_{PEP} did not contribute significantly to the variations of μ/ρ and μ. The incoherent scattering and photoelectric interaction processes involve the incident photons and the electrons of the interaction AW GCs. Consequently, the GCsa with a higher proportion of atoms with a higher atomic number are expected to possess higher values of μ/ρ and μ. Table 1 clearly showed that the introduction of B_2O_3 resulted in a reduction in the weight fraction of denser atoms such as Mg, Al, Si, P, and Ca. Thus μ/ρ and μ decrease for AW GCs with lower B_2O_3 content.

The *HVLs* computed with the aid of **Equation (4)** are plotted as functions of B_2O_3 content and photon energy in Fig. 3. The *HVL* is an vital photon shielding parameter that can be used to assess the thickness of an interacting medium that would allow a specific amount of the incident beam to be transmitted through it. When 50% transmission is of interest, the *HVL* is the thickness of the absorber required. Generally, the required thickness (t) for $\frac{1}{x}$ of the incident beam to be transmitted can be obtained from the *HVL* as:

$$t\ (cm) = HVL\ (cm) \times \log_2 X \quad (11)$$

The *HVL* is therefore an important practical parameter that can be used for gamma radiation shielding designs and calculations. The *HVL* increases with energy due to the reduction in interaction probabilities. At 15 MeV, the *HVL* is about 10.29 cm, 10.36 cm, and 10.53 cm for AW, AW-10B, and AW-20B, respectively. The marginal differences between the *HVL* of the AW GCs show that doping AW with B_2O_3 compromised its photon absorption ability.

A comparison of the photon absorption competence of the AW-20B with different groups of materials is presented in Fig. 4 (a)–(d). In Fig. 4 (a), The mean free path (λ) of AW-20B (the most effective photon absorber among the prepared AW GCs) is placed in contrast to that of RS 360, RS 253 G19, RS 253 G18, RS 253 (Speid, 1991) at three energies, namely, 0.2, 0.662, and 1.25 MeV.

Figure (6b) juxtaposes the λ of AW-20B with some glass systems which have been recommended for radiation shielding applications

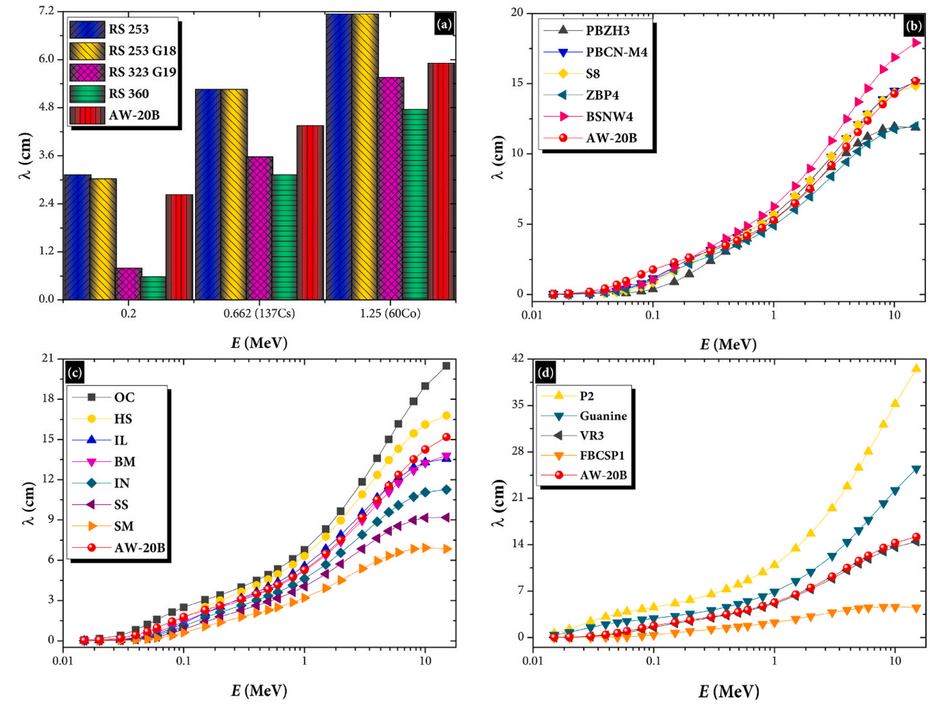

Fig. 4. Comparison of mean free path (λ) parameter of the prepared AW-20B glasses with those in (a) commercial SCHOTT's radiation shielding glasses (Workie et al., 2023), (b) some glass systems (Oonishi et al., 1999; Al- et al., 2022a; Rammah et al., 2021; Sola et al., 2023; Yamamuro, 2016), (c) standard shielding concretes (Kokubo et al., 1982), and (d) polymer-composite materials (Li et al., 1991; Shih et al., 2010; Da Li et al., 2009; Rattanachan et al., 2012).

namely, PBZH3 (Alharshan et al., 2022a), PBCN-M4 (Alharshan et al., 2022b), S8 (Singh et al., 2022), ZBP4 (Alothman et al., 2021), and BSNW4 (Al- et al., 2021d) in a wide (15–15000 keV) energy spectrum. It is clear that AW-20B has photon shielding ability better than BSNW4 and comparable to S8. The chemical composition of the different materials is responsible for the variations in their λ. Concrete is a traditional biological shield. In the past, the shielding capacity of concrete has been improved through the addition of dense aggregates. Hence different concrete samples with varying shielding competences have been produced and analyzed in the past (Bashter, 1997). In Fig. 4 (c), the shielding efficacy (in terms of λ) of different shielding concrete species including ((Concretes; ordinary (OC), hematite-serpentine (HS), ilmenite-limonite (IL), basalt-magnetite (BM), ilmenite (IN), steel-scrap (SS), and steel-magnetite (SM) concretes) [**38**] is compared to AW-20B. The figure shows that AW-20B can absorb photons better than OC and HS. In addition, IL has an almost equal λ with AW-20B, especially at energies below 6 MeV. The density of the various materials played a major role in delineating the λ as seen in Fig. 4 (c). Finally, the comparison of the shielding competence of AW-20B with different classes of materials is presented in Fig. 4 (d). The compared materials include P2 polymer (Al- et al., 2021), Guanine nucleobase (Al- et al., 2021e), VR3 rock (Saeed et al., 2021), and FBCSP1 alloy (Alshahrani et al., 2021). It is obvious that AW-20B can absorb photons better than P2 and guanine. Also, the shielding ability of VR3 is similar to that AW-20B. FBCSP1 however had a better absorption ability for photons compared to AW-20B due to its higher density and composition.

The effective atomic number (Z_{eff}), and effective electron density (N_{eff}) are two parameters that are commonly used to investigate how well a material interacts with photon (Podgoršak, 2006; Al- et al., 2022c; Sekhar et al., 2021; Al- et al., 2022d; Singh et al., 2021; Al- et al., 2022e). Both parameters are more sensitive to changes in chemical composition than the previously discussed parameters. While Z_{eff} represents the number of electrons present in a composite material and available for interactions, N_{eff} represents the number of electrons per unit mass in a composite material. The value Z_{eff} for AW, AW-10B, and AW-20B are plotted against energy in Fig. 5(a), and are within the range 11.04–17.26, 10.88–17.01, and 10.21–16.72, respectively. The effective number of electrons in the AW GCs decline in number as the amount of B_2O_3 increases. This can be attributed to the decrease in weight proportions of heavier atoms in the AW composite as the B_2O_3 concentration rises. Conversely, Fig. 5(b) indicated that N_{eff} follows an inverse trend as Z_{eff}. Generally, the $Z/_{A}$ term in Equation (7) decreases with Z, hence, the observed trend. In addition, the term is almost constant for energy region where incoherent scattering of photons is significant. This clearly explain the nearly constant value of N_{eff} for energies above 0.1 MeV.

The aforementioned attenuation parameters describe the interaction of photons, however, when the interest is the amount of energy deposits in the interacting medium, other parameters such as the mass energy absorption coefficient ($\frac{\mu_{en}}{\rho}$), specific gamma constant, Γ, and absorbed dose rate (D_r) are more appropriate. During interaction, photons transfer part of their energy to the interacting medium, a proportion of this energy is then absorbed by the medium. The probability of interaction (μ/ρ) is related to that of absorption ($\frac{\mu_{en}}{\rho}$) according to the expression (Podgoršak, 2006):

$$\frac{\mu_{en}}{\rho} = \mu \Big/ \rho \frac{E_{tr}}{E}(1-g) \tag{11}$$

where, E_{tr} measures the amount of energy transferred to charged particles of the interacting medium and g the proportion of the charged particle energy lost to radiation, i.e. the absorbed energy E_{ab}

$$E_{ab} = E_{tr} - E_{rad} = E_{tr}(1-g) \tag{12}$$

Therefore, Equation (11) can be written as:

$$\frac{\mu_{en}}{\rho} = \mu \Big/ \rho \frac{E_{ab}}{E} \tag{13}$$

Since, E_{ab} is usually less than E, $\frac{\mu_{en}}{\rho} < \mu/\rho$ for all E. As expected, $\frac{\mu_{en}}{\rho}$ has minimum and maximum vales at 15 MeV and 15 keV accordingly. The

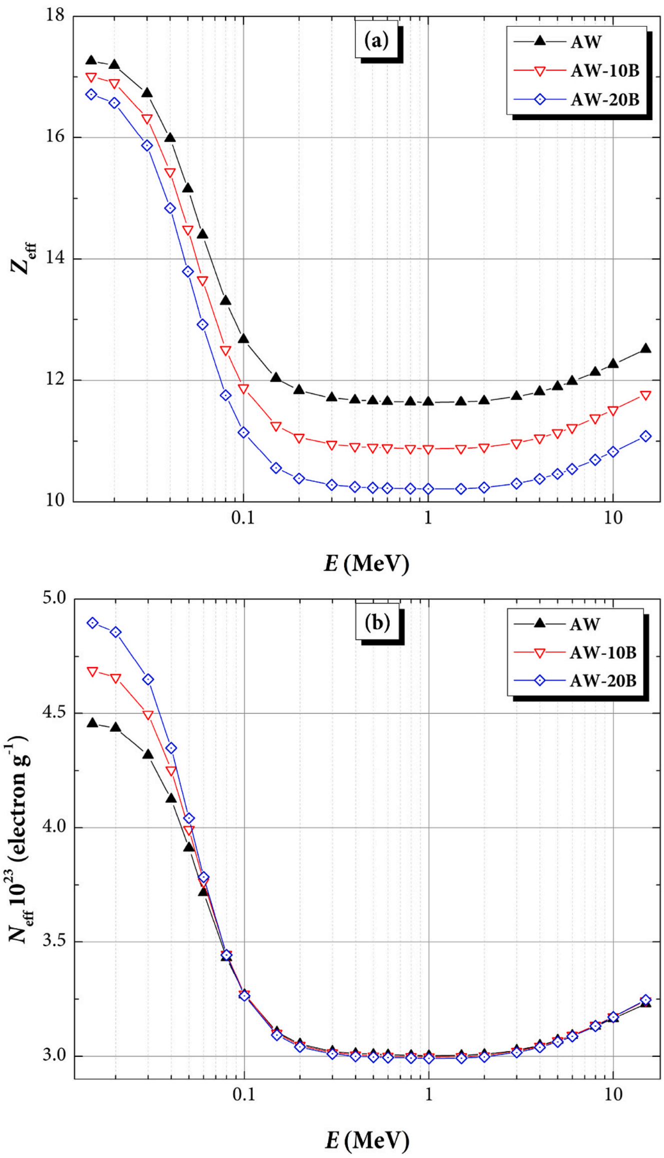

Fig. 5. Variations of (a) effective atomic number and (b) effective electron density of AW-*x*B glasses with different photon energies.

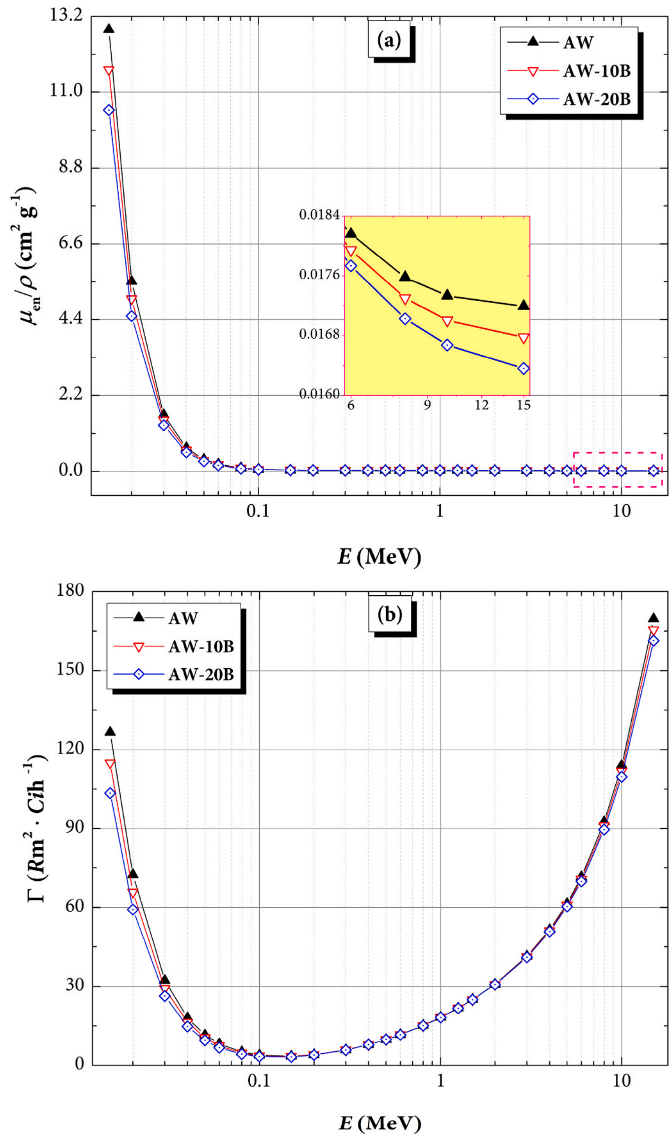

Fig. 6. Variations of (a) mass energy-absorption and (b) specific gamma-ray constant of the prepared AW-*x*B glasses with different photon energies.

minimum and maximum values correspond to 0.0172 and 12.8200 cm^2/g for AW, 0.0168 and cm^2/g for AW-10B, and 0.0164 and 10.4858 cm^2/g for AW-20B. Fig. 6(a) shows how $\frac{\mu_{en}}{\rho}$ changes with E for pristine and doped AW samples. By virtue of Equation (13), the trend of $\frac{\mu_{en}}{\rho}$ is similar to that of μ/ρ for the same reasons. Therefore, the gamma energy absorbed by the AW GCs decreases as the doping concentration of B_2O_3.

The specific gamma constant Γ is a normalized absorbed dose due to a radioactive source at 1 m away from an absorbing medium. in Fig. 6 (b), in view of high photon absorption due to photoelectric absorption and high ionization due to high energies, Γ is high at the low and high end of the energy range respectively. Relatively, the value of Γ decreases slightly as the doping load of B_2O_3 increases in the AW GCs. This is a result of the decline in $\frac{\mu_{en}}{\rho}$.

The absorbed gamma dose rate (D_r) in the AW samples was estimated at sample depth of 1 mm, 5 mm, 10 mm, and 15 mm and presented as functions of E in Fig. 7. Due to exponential and geometric attenuation of photons and absorbed energy, the value of D_r are highest at smaller depths and vice versa. The energy variations of D_r are significantly influenced by $\frac{\mu_{en}}{\rho}$ and Γ. When photons are scattered, depending on the thickness of the interacting medium, the secondary photons can multiply or buildup. Photon scattering leading to buildup are undesirable in shielding scenarios because it compromises shielding. In many practical situations buildup could be significant, hence it is essential to analyse a medium in terms of photon scattering or buildup capacity. High photon buildup is associated with low shielding competence. First, the equivalent atomic number (Z_{eq}) was computed for the GCs. second, the energy absorption (EABF) and exposure (EBF) buildup factors were computed. The equivalent Z compares the photon scattering competence of a composite material with that of a pure atom. For the present materials, the Z_{eq} ranged from 13.61, 12.96, and 12.31 to 15.28, 14.20, and 13.76, for AW, AW-10B, and AW-20B, respectively. The changes in the value of Z_{eq} with photon energy is demonstrated in Fig. 8. The highest values of Z_{eq} were observed at energies where incoherent scattering is maximum, as expected. In addition, Z_{eq} decreases with increase in the B_2O_3 concentration. Figs. 9 and 10 demonstrate plots of EABF and EBF as functions of photon energy and B_2O_3 content of the GCs for selected thickness within 40 mfp. Higher buildup factors were recorded at greater depths due to multiple scattering of incident and secondary photons. Based on the buildup factors, the photon buildup and scattering potentials of the GCs increases with B_2O_3. Clearly, the addition of B_2O_3

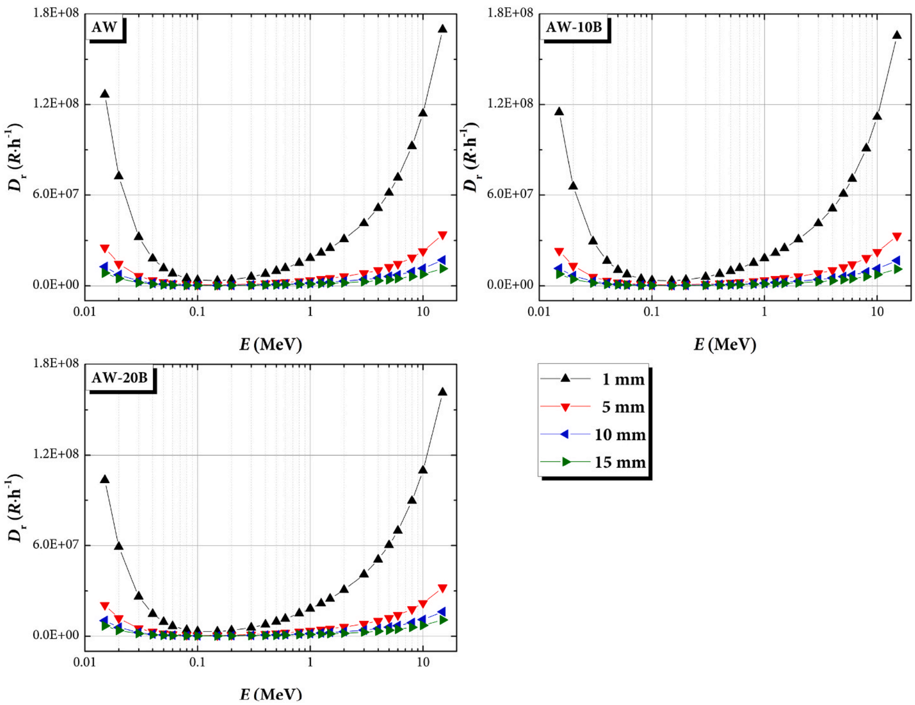

Fig. 7. Variation of gamma dose rate at different photon energy levels for the prepared AW-*x*B glasses.

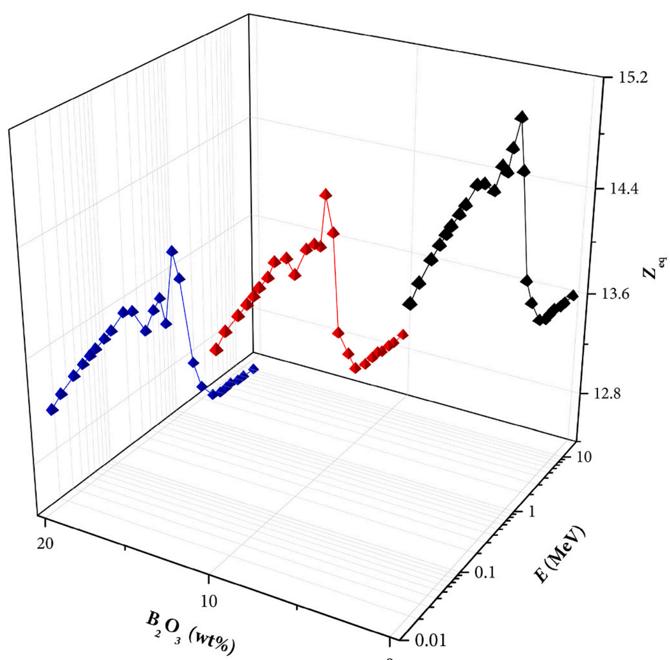

Fig. 8. Variation of equivalent atomic number with respect to the concentration of B_2O_3 and a function of photon energy in the prepared AW-*x*B glasses.

compromised the photon shielding competence of AW in both narrow beam and broad beam scenarios. Such findings support our previous works including different materials, especially glasses, doping with different heavy metal oxides (Alzahrani et al., 2021; Al- et al., 2022f; Al-and Buriahi, 2023; Alzahrani et al., 2024; Alzahrani et al., 2023b; Alalawi et al., 2023; Katubi et al., 2023; Alzahrani et al., 2023c).

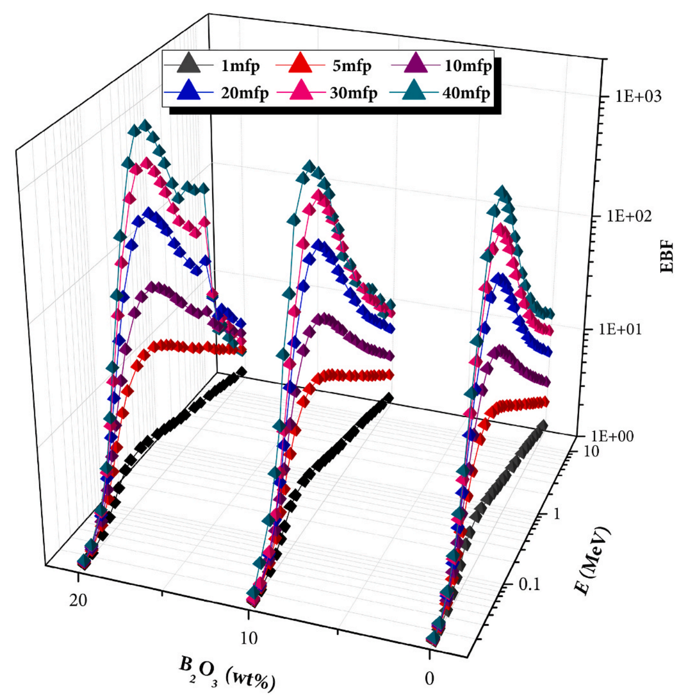

Fig. 9. Variation of exposure buildup factor (EBF) with respect to the concentration of B_2O_3 and a function of photon energy in the prepared AW-*x*B glasses.

4. Conclusion

In the research, B_2O_3-doped AW GCs were synthesized, and their density and hardness were measured. In addition, the influence of dopant concentration on the photon interaction parameters of the GCs for a wide photon energy spectrum was investigated using Monte Carlo simulations and standard calculations. The introduction of B_2O_3 resulted

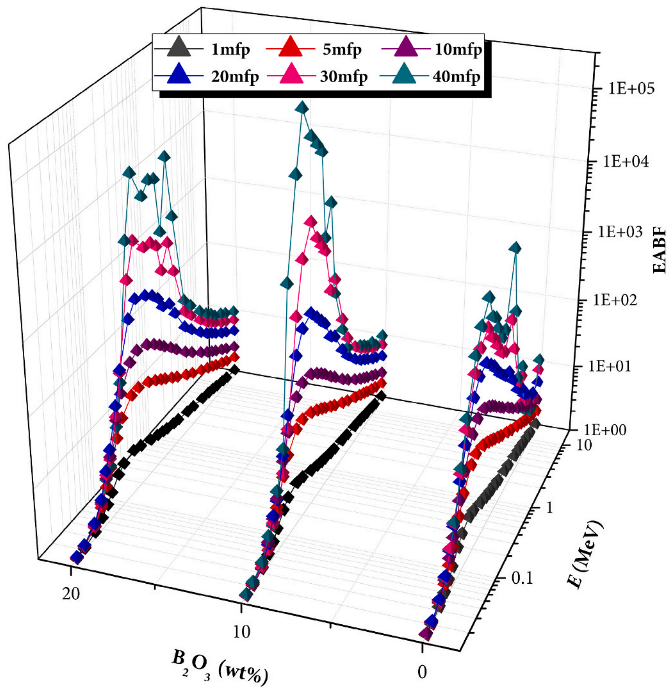

Fig. 10. Variation of energy absorption buildup factor (EABF) with respect to the concentration of B_2O_3 and a function of photon energy in the prepared AW-*x*B glasses.

in a reduction in the weight fraction of denser atoms such as Mg, Al, Si, P, and Ca. The corresponding densities were 2.905, 2.957, and 2.986 g/cm^3, respectively. The mass attenuation coefficients were found to be within the ranges 0.0231–13.5659 cm^2/g, 0.0225–12.3561 cm^2/g, and 0.0220–11.1079 cm^2/g for AW, AW-10B, and AW-20B, respectively. The effective atomic number of the GCs fell within the ranges 11.04–17.26, 10.88–17.01, and 10.21–16.72, respectively. The Z_{eq} ranged from 13.61, 12.96, and 12.31 to 15.28, 14.20, and 13.76, for AW, AW-10B, and AW-20B, respectively. Doping AW with B_2O_3 compromised its photon absorbing and shielding competence. The GCs had better photon-absorbing competence than some existing gamma-photon shields. The GCs could be used as radiation absorbers; however, radiation damage to the materials should be investigated before field deployment for shielding or related applications.

CRediT authorship contribution statement

Norah Alomayrah: Supervision and Review.
Marzoqa. M. Alnairi: Supervision and Support.
Z.A. Alrowaili: Supervision and Support.
B. Alshahrani: Supervision and support.
Mine Kirkbinar: Support.
I.O. Olarinoye: Formal analysis and writing the original draft.
Halil Arslan: Supervision.
M.S. Al-Buriahi: Conceptualization, Writing - Review and Editing.

Declaration of competing interest

We have no conflict of interest to declare.

Data availability

No data was used for the research described in the article.

Acknowledgement

The authors express their gratitude to Princess Nourah bint Abdulrahman University Researchers Supporting Project number (PNURSP2024R450), Princess Nourah bint Abdulrahman University, Riyadh, Saudi Arabia. Moreover, the authors extend their appreciation to the Deanship of Scientific Research at King Khalid University, Saudi Arabia for funding this work through Large Groups Project under grant number R.G.P2/74/44.

References

Al-Buriahi, M.S., 2023. Radiation shielding performance of a borate-based glass system doped with bismuth oxide. Radiat. Phys. Chem. 207, 110875.
Al-Buriahi, Sultan, Mohammed, Gaikwad, Dhammajyot Kundlik, Hegazy, H.H., Sriwunkum, Chahkrit, Neffati, R., 2021a. Fe-based alloys and their shielding properties against directly and indirectly ionizing radiation by using FLUKA simulations. Phys. Scripta 96 (4), 045303.
Al-Buriahi, M.S., Olarinoye, I.O., Alomairy, S., Kebaili, I., Kaya, R., Arslan, H., Tonguc, B. T., 2021b. Dense and environment friendly bismuth barium telluroborate glasses for nuclear protection applications. Prog. Nucl. Energy 137, 103763.
Al-Buriahi, Sultan, Mohammed, Alzahrani, Jamila S., Olarinoye, I.O., Akyildirim, Hakan, Alomairy, Sultan, Kebaili, Imen, Tekin, H.O., Mutuwong, Chalermpon, 2021c. Role of heavy metal oxides on the radiation attenuation properties of newly developed TBBE-X glasses by computational methods. Phys. Scripta 96 (7), 075302.
Al-Buriahi, M.S., Taha, T.A., Alothman, M.A., Donya, H., Olarinoye, I.O., 2021d. Influence of WO3 incorporation on synthesis, optical, elastic and radiation shielding properties of borosilicate glass system. Eur. Phys.J. Plus 136 (7), 779.
Al-Buriahi, M.S., Sriwunkum, C., Boukhris, I., 2021e. X-and gamma-rays attenuation properties of DNA nucleobases by using FLUKA simulation code. Eur. Phys.J. Plus 136 (7), 776.
Al-Buriahi, M.S., Alrowaili, Z.A., Eke, C., Alomairy, S., Alshahrani, B., Bejaoui, I., Sriwunkum, C., 2022a. An important role of Ba2+, Sr2+, Mg2+, and Zn2+ in the radiation attenuation performance of CFCBPC bioactive glasses. J. Austral.Ceram. Soc. 58 (2), 461–473.
Al-Buriahi, M.S., Alrowaili, Z.A., Alsufyani, Sultan J., Olarinoye, I.O., Alharbi, Abdulaziz N., Sriwunkum, Chahkrit, Kebaili, Imen, 2022b. The role of PbF2 on the gamma-ray photon, charged particles, and neutron shielding prowess of novel lead fluoro bismuth borate glasses. J. Mater. Sci. Mater. Electron. 33 (3), 1123–1139.
Al-Buriahi, M.S., Alrowaili, Z.A., Eke, Canel, Alzahrani, Jamila S., Olarinoye, I.O., Chahkrit, Sriwunkum, 2022c. Optical and radiation shielding studies on tellurite glass system containing ZnO and Na2O. Optik 257, 168821.
Al-Buriahi, M.S., Hessien, Manal, Alresheedi, Faisal, Al-Baradi, Ateyyah M., Alrowaili, Z. A., Kebaili, Imen, Olarinoye, I.O., 2022d. ZnO–Bi2O3 nanopowders: fabrication, structural, optical, and radiation shielding properties. Ceram. Int. 48 (3), 3464–3472.
Al-Buriahi, M.S., Alrowaili, Z.A., Eke, Canel, Alomairy, Sultan, Alshahrani, B., Bejaoui, Imen, Sriwunkum, Chahkrit, 2022e. An important role of Ba2+, Sr2+, Mg2 +, and Zn2+ in the radiation attenuation performance of CFCBPC bioactive glasses. J. Austral.Ceram. Soc. 58 (2), 461–473.
Al-Buriahi, M.S., Alrowaili, Z.A., Alomairy, Sultan, Olarinoye, I.O., Chalermpon, Mutuwong, 2022f. Optical properties and radiation shielding competence of Bi/Te-BGe glass system containing B2O3 and GeO2. Optik 257, 168883.
Alalawi, Amani, Al-Buriahi, Mohammed Sultan, Sayyed, M.I., Akyildirim, H., Arslan, Halil, Zaid, M.H.M., Tonguç, Barış T., 2020. Influence of lead and zinc oxides on the radiation shielding properties of tellurite glass systems. Ceram. Int. 46 (11), 17300–17306.
Alalawi, Amani, Huwayz, Maryam Al, Alrowaili, Z.A., Al-Buriahi, M.S., 2023. Radiation attenuation of SiO2–MgO glass system for shielding applications. J. Radiat. Res. Appl. Sci. 16 (4), 100746.
Alharshan, G.A., Alrowaili, Z.A., Olarinoye, I.O., Al-Buriahi, M.S., 2022a. Holmium (III) oxide and its significant effects on the radiation shielding performance of P2O5+ B2O3+ ZnSO4 optical glasses. Optik 261, 169188.
Alharshan, G.A., Alrowaili, Z.A., Olarinoye, I.O., Sriwunkum, C., Tonguc, B.T., Al-Buriahi, M.S., 2022b. Optical borophosphate glass system with excellent properties for radiation shielding applications. Optik 266, 169568.
Alothman, M.A., Alrowaili, Z.A., Al-Baradi, A.M., Kilicoglu, O., Mutuwong, C., Al-Buriahi, M.S., 2021. Elastic properties and radiation shielding ability of ZnO–P2O5/B2O3 glass system. J. Mater. Sci. Mater. Electron. 32 (14), 19203–19217.
Alshahrani, B., Olarinoye, I.O., Mutuwong, C., Sriwunkum, C., Yakout, H.A., Tekin, H.O., Al-Buriahi, M.S., 2021. Amorphous alloys with high Fe content for radiation shielding applications. Radiat. Phys. Chem. 183, 109386.
Alzahrani, Jamila S., Alrowaili, Z.A., Olarinoye, I.O., Alothman, Miysoon A., Al-Baradi, Ateyyah M., Kebaili, Imen, Al-Buriahi, M.S., 2021. Nuclear shielding properties and buildup factors of Cr-based ferroalloys. Prog. Nucl. Energy 141, 103956.
Alzahrani, Jamila S., Alrowaili, Z.A., Eke, Canel, Mahmoud, Zakaria MM., Mutuwong, C., Al-Buriahi, M.S., 2022. Nuclear shielding properties of Ni-, Fe-, Pb-, and W-based alloys. Radiat. Phys. Chem. 195, 110090.

Alzahrani, F.M.A., Albarkaty, K.S., Çalişkan, F., Olarinoye, I.O., Al-Buriahi, M.S., 2023a. Physical, microstructural, and radiation energy absorption properties of recycled CRT-screen glass doped with Bi2O3. J. Radiat. Res. Appl. Sci. 16 (4), 100727.

Alzahrani, J.S., Alrowaili, Z.A., Chandra Sekhar, K., Olarinoye, I.O., Sriwunkum, Chahkrit, Alalawi, Amani, Al-Buriahi, M.S., 2023b. Synthesis and optimization of alkaline earth borate glasses doped with Fe2O3: significance of BaO/MgO on the physical, structural features and radiation shielding performance. J. Radiat. Res. Appl. Sci. 16 (4), 100747.

Alzahrani, Jamila S., Yilmaz, Ebru, Çalişkan, Fatih, Alrowaili, Z.A., Olarinoye, I.O., Alqahtani, Mohammed S., Arslan, Halil, Al-Buriahi, M.S., 2023c. Synthesis and optimization of B2O3-based glass: influence of MgO on hardness, structure properties, and radiation shielding performance. Mater. Today Commun. 37, 106933.

Alzahrani, Fatimah Mohammed, A., Elqahtani, Zainab Mufarreh, Alzahrani, Jamila S., Eke, Canel, Alrowaili, Z.A., Al-Buriahi, M.S., 2024. Gamma attenuation characteristics of silicon-rich glasses in Na2O–SiO2–Al2O3–CaO–ZnO system for radiation applications. J. Radiat. Res. Appl. Sci. 17 (1), 100760.

Al Buriahi, M.S., Eke, C., Alomairy, S., Yildirim, A., Alsaeedy, H.I., Sriwunkum, C., 2021. Radiation attenuation properties of some commercial polymers for advanced shielding applications at low energies. Polym. Adv. Technol. 32 (6), 2386–2396.

Bashter, I.I., 1997. Calculation of radiation attenuation coefficients for shielding concretes. Ann. Nucl. Energy 24 (17), 1389–1401.

Berger, M.J., 2010. NIST XCOM: Photon Cross Sections Database nist. gov/pml/data/xcom/index. cfm.

Da Li, G., Pan, T.H., Chen, G.S., Lin, Y., Mao, M., Yan, G., 2009. Effect of Mn–Zn ferrite on apatite–wollastonite glass-ceramic (A–W GC). Biomed. Mater. 4 (4), 045001.

Jing, H., Gan, T., Tang, X., & Li, F. Effect of Titanium Addition on Physicochemical and Biological Properties of Apatite-Wollastonite Glass Ceramic. .

Katubi, Mohammedsaleh, Khadijah, Basha, Beriham, Alsufyani, Sultan J., Alrowaili, Z.A., Sriwunkum, Chahkrit, Alnairi, Marzoqa M., Al-Buriahi, M.S., 2023. Radiation attenuation and optical properties of P2O5-based glass system. J. Radiat. Res. Appl. Sci. 16 (4), 100688.

Kitsugi, T., Yamamuro, T., Nakamura, T., Yoshii, S., Kokubo, T., Takagi, M., Shibuya, T., 1992. Influence of substituting B2O3 for CaF2 on the bonding behaviour to bone of glass-ceramics containing apatite and wollastonite. Biomaterials 13 (6), 393–399.

Kokubo, T., Shigematsu, M., Nagashima, Y., Tashiro, M., Nakamura, T., Yamamuro, T., Higashi, S., 1982. Apatite-and wollastonite-containg glass-ceramics for prosthetic application. Bull. Inst. Chem. Res. Kyoto Univ. 60 (3–4), 260–268.

Li, R., Clark, A.E., Hench, L.L., 1991. An investigation of bioactive glass powders by sol-gel processing. J. Appl. Biomater. 2 (4), 231–239.

Menazea, A.A., Abdelghany, A.M., 2020. Gamma irradiated Hench's Bioglass and their derivatives Hench's Bioglass-ceramic for bone bonding efficiency. Radiat. Phys. Chem. 174, 108932.

Ogundare, F.O., Olarinoye, I.O., 2016. He+ induced changes in the surface structure and optical properties of RF-sputtered amorphous alumina thin films. J. Non-Cryst. Solids 432, 292–299.

Olarinoye, I.O., Ogundare, F.O., 2017. Optical and microstructural properties of neutron irradiated RF-sputtered amorphous alumina thin films. Optik 134, 66–77.

Olarinoye, I.O., Odiaga, R.I., Paul, S., 2019. EXABCal: a program for calculating photon exposure and energy absorption buildup factors. Heliyon 5 (7), e02017.

Olarinoye, I.O., Rammah, Y.S., Alraddadi, Shoroog, Sriwunkum, Chahkrit, Abd El-Rehim, A.F., Zahran, H.Y., Al-Buriahi, M.S., 2020. The effects of La2O3 addition on mechanical and nuclear shielding properties for zinc borate glasses using Monte Carlo simulation. Ceram. Int. 46 (18), 29191–29198.

Olarinoye, I.O., Alomairy, S., Sriwunkum, C., Al-Buriahi, M.S., 2021. Effect of Ag2O/V2O5 substitution on the radiation shielding ability of tellurite glass system via XCOM approach and FLUKA simulations. Phys. Scripta 96 (6), 065308.

Oonishi, H., Hench, L.L., Wilson, J., Sugihara, F., Tsuji, E., Kushitani, S., Iwaki, H., 1999. Comparative bone growth behavior in granules of bioceramic materials of various sizes. J. Biomed. Mater. Res.: Off. J. Soc. Biomater.Japan.Soc.Biomater., Austral. Soc. Biomater. 44 (1), 31–43.

Podgoršak, E.B., 2006. Radiation Physics for Medical Physicists, vol. 1. Springer, Berlin.

Rammah, Y.S., Olarinoye, I.O., El-Agawany, F.I., Ibrahim, S., Ali, A.A., 2021. SrO-reinforced potassium sodium borophosphate bioactive glasses: compositional, physical, spectral, structural properties and photon attenuation competence. J. Non-Cryst. Solids 559, 120667.

Rattanachan, S.T., Srakaew, N., Pethnin, R., Suppakarn, N., 2012. Effect of Zn addition on sol-gel derived apatite/wollastonite glass-ceramics scaffolds. J. Metals, Mater. Min. 22 (2).

Saeed, A., Alomairy, S., Sriwunkum, C., Al-Buriahi, M.S., 2021. Neutron and charged particle attenuation properties of volcanic rocks. Radiat. Phys. Chem. 184, 109454.

Samdani, M., Basha, B., Alsufyani, S.J., Kebaili, I., Sekhar, K.C., Alrowaili, Z.A., et al., 2024. Gamma shielding performance of B2O3/BaO-based glassy system: synthesis and simulation study. Radiat. Phys. Chem. 214, 111301.

Sekhar, Chandra, K., Narsimlu, N., Al-Buriahi, M.S., Yakout, H.A., Olarinoye, I.O., Alomairy, Sultan, Shareefuddin, M.D., 2021. Synthesis, optical, and radiation attenuation properties of CaF2-TeO2-Na2B4O7-CuO glass system for advanced shielding applications. Eur. Phys.J. Plus 136 (9), 903.

Shih, C.J., Chen, H.T., Huang, L.F., Lu, P.S., Chang, H.F., Chang, I.L., 2010. Synthesis and in vitro bioactivity of mesoporous bioactive glass scaffolds. Mater. Sci. Eng. C 30 (5), 657–663.

Singh, Jagpreet, Kumar, Vishal, Vermani, Yogesh K., Al-Buriahi, M.S., Alzahrani, Jamila S., Singh, Tejbir, 2021. Fabrication and characterization of barium based bioactive glasses in terms of physical, structural, mechanical and radiation shielding properties. Ceram. Int. 47 (15), 21730–21743.

Singh, J., Kaur, P., Kaur, P., Kumar, V., Al-Buriahi, M.S., Alfryyan, N., et al., 2022. Optical and radiation shielding features for some phospho-silicate glasses. Optik 261, 169140.

Sola, D., Chueca, E., Wang, S., Peña, J.I., 2023. Surface activation of calcium zirconate-calcium stabilized zirconia eutectic ceramics with bioactive wollastonite-tricalcium phosphate coatings. J. Funct. Biomater. 14 (10), 510.

Speid, B., 1991. Radiation-shielding glasses providing safety against electrical discharge and being resistant to discoloration. Google Patents. https://patents.google.com/patent/US5073524A/en. (Accessed 8 March 2023).

Świontek, S., Środa, M., Gieszczyk, W., 2021. Ceramics, glass and glass-ceramics for personal radiation detectors. Materials 14 (20), 5987.

Workie, A.B., Ningsih, H.S., Yeh, W.L., Shih, S.J., 2023. An investigation of in vitro bioactivities and cytotoxicities of spray pyrolyzed apatite wollastonite glass-ceramics. Crystals 13 (7), 1049.

Yamamuro, T., 2016. Clinical application of glass ceramics. Biomechan. Biomater. Orthoped. 153–157.

Yang, X., Zhang, L., Chen, X., Sun, X., Yang, G., Guo, X., et al., 2012. Incorporation of B2O3 in CaO-SiO2-P2O5 bioactive glass system for improving strength of low-temperature co-fired porous glass ceramics. J. Non-Cryst. Solids 358 (9), 1171–1179.

Yoshida, Y., 2006. Development of fitting methods using geometric progression formulae of gamma-ray buildup factors. J. Nucl. Sci. Technol. 43 (12), 1446–1457.